RESEARCH ARTICLE

Superresolution Imaging Captures Carbohydrate Utilization Dynamics in Human Gut Symbionts

Krishanthi S. Karunatilaka,[a]* Elizabeth A. Cameron,[b] Eric C. Martens,[b] Nicole M. Koropatkin,[b] Julie S. Biteen[a]

Department of Chemistry, University of Michigan, Ann Arbor, Michigan, USA[a]; Department of Microbiology and Immunology, University of Michigan Medical School, Ann Arbor, Michigan, USA[b]

* Present address: Krishanthi S. Karunatilaka, Department of Biological Chemistry and Molecular Pharmacology, Harvard Medical School, Boston, Massachusetts, USA.

ABSTRACT **Gut microbes play a key role in human health and nutrition by catabolizing a wide variety of glycans via enzymatic activities that are not encoded in the human genome. The ability to recognize and process carbohydrates strongly influences the structure of the gut microbial community. While the effects of diet on the microbiota are well documented, little is known about the molecular processes driving metabolism. To provide mechanistic insight into carbohydrate catabolism in gut symbionts, we studied starch processing in real time in the model *Bacteroides thetaiotaomicron* starch utilization system (Sus) by single-molecule fluorescence. Although previous studies have explored Sus protein structure and function, the transient interactions, assembly, and collaboration of these outer membrane proteins have not yet been elucidated in live cells. Our live-cell superresolution imaging reveals that the polymeric starch substrate dynamically recruits Sus proteins, serving as an external scaffold for bacterial membrane assembly of the Sus complex, which may promote efficient capturing and degradation of starch. Furthermore, by simultaneously localizing multiple Sus outer membrane proteins on the *B. thetaiotaomicron* cell surface, we have characterized the dynamics and stoichiometry of starch-induced Sus complex assembly on the molecular scale. Finally, based on Sus protein knockout strains, we have discerned the mechanism of starch-induced Sus complex assembly in live anaerobic cells with nanometer-scale resolution. Our insights into the starch-induced outer membrane protein assembly central to this conserved nutrient uptake mechanism pave the way for the development of dietary or pharmaceutical therapies to control *Bacteroidetes* in the intestinal tract to enhance human health and treat disease.**

IMPORTANCE **In this study, we used nanometer-scale superresolution imaging to reveal dynamic interactions between the proteins involved in starch processing by the prominent human gut symbiont *Bacteroides thetaiotaomicron* in real time in live cells. These results represent the first working model of starch utilization system (Sus) complex assembly and function during glycan catabolism and are likely to describe aspects of how other Sus-like systems function in human gut *Bacteroidetes*. Our results provide unique mechanistic insights into a glycan catabolism strategy that is prevalent within the human gut microbial community. Proper understanding of this conserved nutrient uptake mechanism is essential for the development of dietary or pharmaceutical therapies to control intestinal tract microbial populations, to enhance human health, and to treat disease.**

Received 18 October 2014 **Accepted** 21 October 2014 **Published** 11 November 2014

Citation Karunatilaka KS, Cameron EA, Martens EC, Koropatkin NM, Biteen JS. 2014. Superresolution imaging captures carbohydrate utilization dynamics in human gut symbionts. mBio 5(6):e02172-14. doi:10.1128/mBio.02172-14.

Invited Editor Kerwyn Casey Huang, Stanford University **Editor** Edward G. Ruby, University of Wisconsin-Madison

Address correspondence to Julie S. Biteen, jsbiteen@umich.edu.

The human gut contains trillions of densely colonizing bacteria that directly influence our health (1). The majority of these symbionts have a beneficial relationship with humans and promote the degradation of host-indigestible complex glycans, producing short-chain fatty acids that can be utilized by both microbes and humans (2, 3). To efficiently compete for both dietary and host-derived mucosal glycans, gut microbes have evolved a number of different strategies that allow them to scavenge nutrients in the densely populated human gut (1, 4).

Bacteroides thetaiotaomicron, a prominent Gram-negative anaerobic bacterial symbiont in the human gut, metabolizes over a dozen different glycans (5, 6). The starch utilization system (Sus) is a well-known multiprotein system that is essential for *B. thetaiotaomicron* to catabolize starch, a large glucose polymer that is abundant in the human diet. Sus consists of eight proteins, SusRABCDEFG (Fig. 1) (7), the last five of which are involved in starch acquisition at the cell surface. Based on previous biochemical, structural, and genetic analyses, the outer membrane-associated proteins SusCDEF assist starch binding to the cell surface (8–12), while the α-amylase SusG degrades starch into smaller oligosaccharides (13, 14). SusC, a TonB-dependent transporter, imports these oligosaccharides to the periplasm for further degradation into mono- and disaccharides by SusA and SusB (5, 15). The SusR transcriptional regulator activates Sus expression in the presence of starch or starch derivatives such as the disaccharide maltose (16). Similarly patterned protein systems, termed Sus-like systems, comprise ~18% of the *B. thetaiotaomicron* genome and have been identified in all sequenced gut members of

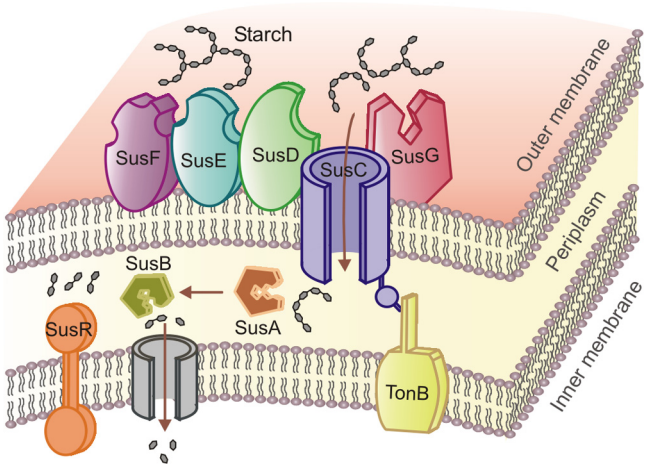

FIG 1 Model for starch catabolism by the *B. thetaiotaomicron* Sus. The Sus consists of eight proteins (SusRABCDEFG), including five outer membrane-associated proteins that promote starch binding, degradation, and import. The exact interactions among these proteins and their stoichiometry have not been elucidated with conventional techniques, but nine sites that interact with starch have been discovered by protein structure determination (12).

the *Bacteroidetes* (17), making the *B. thetaiotaomicron* Sus an important model for studying glycan acquisition by gut bacteria.

Although previous studies have explored Sus protein structure and function, the interactions and assembly of these outer membrane proteins (OMPs) in live cells have not yet been elucidated. Formaldehyde cross-linking and nondenaturing gel electrophoresis studies have shown evidence for SusC/SusD interactions (9). Furthermore, SusE appears to interact with both SusF and SusCD, forming an OMP complex (9). Together, these ensemble studies provide a static picture of putative protein associations but do not reveal the transient interactions that occur during starch catabolism in cells. Therefore, to reveal the precise mechanisms of Sus protein assembly and collaboration during starch processing, we monitored Sus proteins and their dynamic interactions in real time in live microbes.

Fluorescent labeling of proteins is invaluable for studying intracellular biology (18, 19). Despite the power of fluorescence imaging to explore complex biological systems, standard optical microscopy is unable to fully resolve dynamics and biomolecular interactions on length scales smaller than the ~0.5-μm diffraction limit (20, 21). To overcome the resolution barrier and to reveal the assembly and real-time dynamics of the Sus OMPs under anaerobic conditions, we applied single-molecule superresolution imaging to fluorophore-labeled Sus proteins (20). Two-color single-molecule imaging of fluorescently tagged starch substrates and SusG, an enzyme required for starch catabolism (13), enabled the direct observation of interactions between starch and SusG during starch processing in live *B. thetaiotaomicron*. Furthermore, by simultaneously localizing multiple Sus OMPs in the presence of starch on the *B. thetaiotaomicron* cell surface, we characterized starch-induced Sus complex assembly with nanometer-scale resolution. Finally, based on Sus protein knockout strains, the mechanism of starch-induced Sus complex assembly was discerned. In particular, whereas SusG interacts only weakly with other Sus OMPs in the absence of starch, in the presence of starch, SusG dynamically interacts with other Sus proteins to form a stable, starch-induced Sus OMP complex containing at least a single copy of each of the Sus OMPs.

RESULTS

Live-cell imaging of SusG. Fluorescent labeling of proteins presents unique challenges in live-cell imaging of anaerobic bacteria. Most fluorescent proteins (FPs) require oxygen for maturation (22), precluding their use under anaerobic conditions. Recent advances in covalent labeling of proteins with small fluorescent molecules using a fusion partner, such as the HaloTag (HT) protein, provide promising alternatives to FPs (23–25). We applied the HaloTag enzymatic labeling technique to monitor SusG in an oxygen-free environment in live *B. thetaiotaomicron*. To generate the SusG-HT fusion protein, SusG was fused to HT, a modified haloalkane dehalogenase protein (see Fig. S1A in the supplemental material) (14, 24). Comparable growth rates in starch of *B. thetaiotaomicron* containing wild-type SusG (SusG-WT) and *B. thetaiotaomicron* with SusG-HT indicate that this SusG modification has a minimal effect on Sus complex-mediated starch degradation (see Fig. S1B to D).

To determine the positions of SusG on the cell membrane, SusG-HT was fluorescently labeled using a tetramethyl rhodamine (TMR) HT ligand (L). Fluorescent labeling of SusG-HT with this ligand does not significantly affect the *B. thetaiotaomicron* growth rate in starch (see Materials and Methods). Superresolution imaging of fluorophore-labeled SusG-HT (SusG-HTL) in fixed *B. thetaiotaomicron* cells revealed stationary SusG proteins distributed on the cell membrane without specific localizations at any particular location (Fig. 2A and B). To monitor the dynamic behavior of SusG in live cells, it is essential to maintain an oxygen-free environment throughout the imaging time. To overcome this challenge, we assembled live bacterial cells on 2% agarose pads containing minimal medium, a carbohydrate source and a reducing agent between two tightly sealed coverslips (see Fig. S1E in the supplemental material) in an anaerobic chamber (26). Even after the sample was removed from the chamber, cell division was apparent at 37°C in cells assembled as described above (see Fig. S1F), providing an opportunity to track SusG on the membrane in real time in live anaerobes (Fig. 2C and D). Figure 2D shows that SusG-HTL is membrane localized: the increased concentration of fluorescent spots along the cell edges is as expected for the two-dimensional (2D) projection of a cell membrane.

Sus proteins assemble to process starch. A key feature of Sus-like systems is the collective action of multiple proteins during glycan binding and degradation (5). To understand the precise coordinated roles of these proteins during glycan catabolism, we compared the pairwise assembly of Sus OMPs on the cell surface in glucose, which is the monomeric subunit of starch, and in the presence of maize amylopectin (AP), a common plant starch. Concurrent with HaloTag labeling of SusG, protein-specific antibodies (Abs) were used to demarcate each of the Sus OMPs (see Fig. S2A to E in the supplemental material). Comparison of Alexa 488-conjugated-Ab-labeled SusG-WT and SusG-HT (see Fig. S2A and S2B) reveals a similar number of Alexa 488 foci per cell, indicating that the introduction of the HT protein does not impede SusG antibody labeling under these conditions.

As a first step toward understanding Sus complex assembly, SusG-HTL and a second Ab-labeled Sus protein (SusD-, SusE- or SusF-Ab) were simultaneously monitored in fixed cells. The Sus protein positions on the membrane were detected with <20-nm

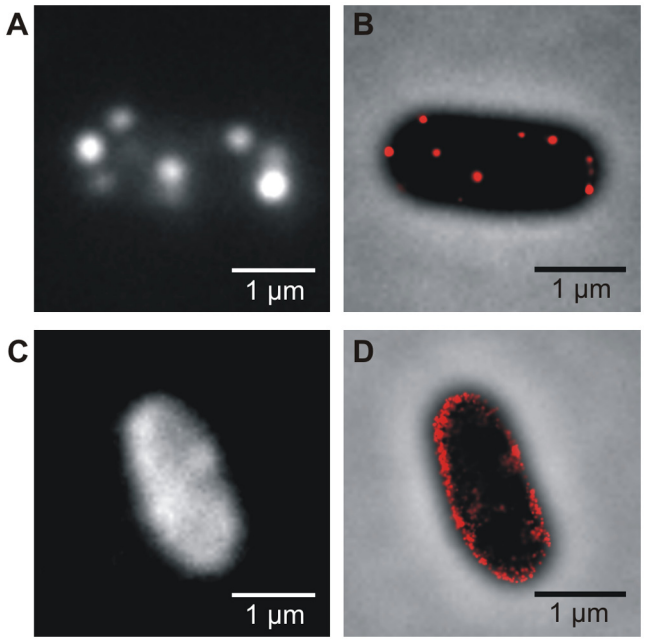

FIG 2 Single-molecule imaging of HaloTag-labeled SusG in glucose-grown *B. thetaiotaomicron*. Diffraction-limited images (A and C) (white) and reconstructed superresolution localization images (B and D) (red) of TMR-HaloTag-labeled SusG in fixed and live cells, respectively. The superresolution images in panels B and D are merged with phase-contrast cell images (black). All images were constructed by stacking imaging frames obtained over time at 10 frames per s. The fixed-cell images show a few discrete spots representing stationary SusG molecules, while the live-cell images include many spots that correspond to a few SusG molecules that were moving on the membrane over time.

precision by fitting the emission intensity profile of individual molecules to a 2D Gaussian function (27). Superresolution images of SusG-HTL and Sus-Ab proteins were reconstructed from these positions to accurately measure protein colocalization. Merged images of reconstructed SusG-HTL (red) and Sus-Ab (green) localizations qualitatively indicate protein assembly (yellow in Fig. 3A to D), although a robust quantitative method is necessary to distinguish differences in Sus protein colocalization with respect to various carbohydrates, as described below.

The colocalization between each pair of biomolecules was quantified by comparing the pixel intensities in superresolution images of each channel with the Pearson correlation coefficient and the Manders coefficients M_{red} and M_{green} (28, 29). The Pearson coefficient measures the linear correlation between two channels and assigns a value to the correlation ranging from −1 (negative correlation) to +1 (positive correlation). The Manders coefficients describe the colocalization of molecules with respect to an individual channel and increase from 0 to 1 with rising colocalization (see Materials and Methods). Antibody labeling was less efficient than HaloTag labeling due to the stringent protocol that we used to prevent nonspecific antibody labeling ($M_{green} = 0.65 \pm 0.03$ and $M_{red} = 0.32 \pm 0.02$ for SusG-HTL and SusG-Ab in glucose); consequently the M_{green} coefficient more accurately represents Sus protein colocalization. In the presence of amylopectin, the Pearson and Manders coefficients indicate higher colocalization levels between SusG and SusD, -E, or -F than in glucose ($P < 0.02$) (Fig. 3E and F; also, see Fig. S2F in the supplemental material). Interestingly, the disaccharide maltose,

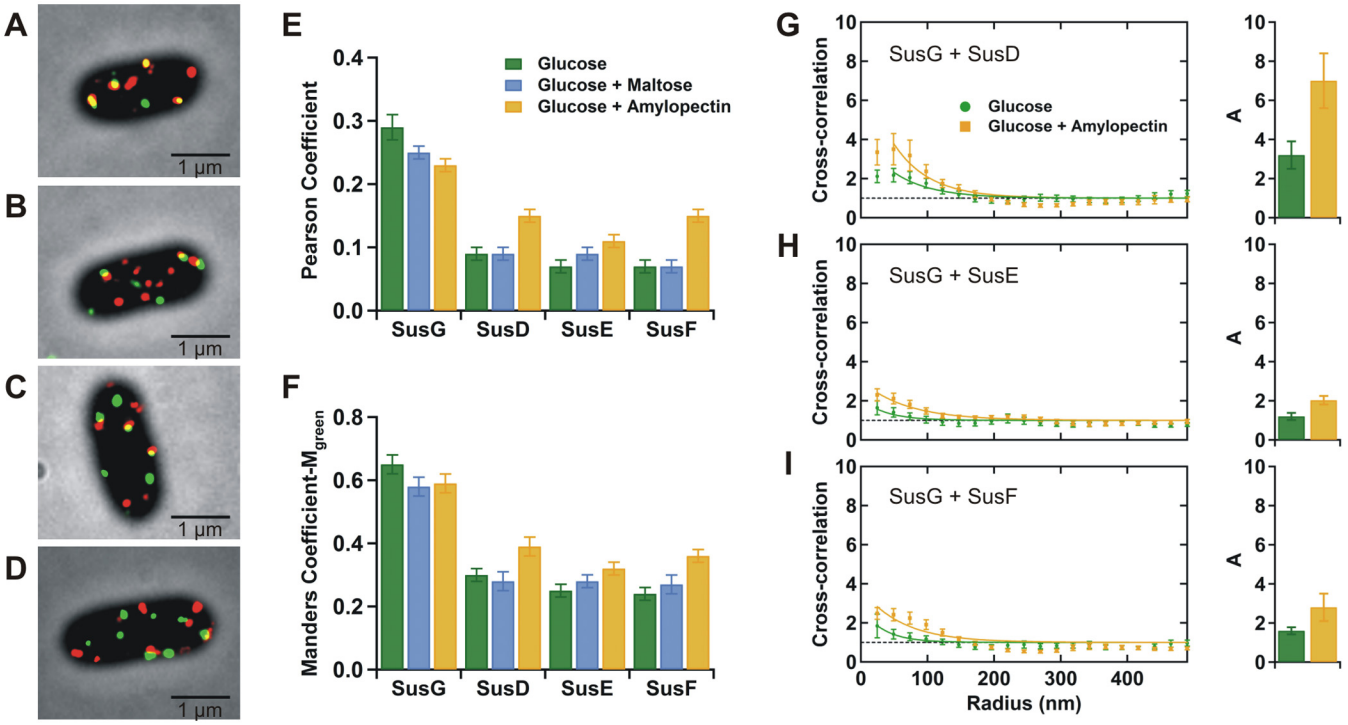

FIG 3 Colocalization of Sus proteins in fixed cells. (A to D) Representative merged superresolution and cell images showing simultaneous localization of SusG-HTL (red) and antibody-labeled SusG, -D, -E, or -F (green), respectively, in glucose-grown *B. thetaiotaomicron*. (E and F) Quantitative analysis of protein colocalization between SusG-HTL and antibody-labeled Sus proteins by Pearson and Manders (M_{green}) coefficients. (G to I) Cross-correlation functions, $c(r)$ (left) and the cross-correlation amplitude (A) obtained from the fit (right) for the indicated Sus protein pairs. The value of $c(r)$ is 1 for random protein localization (black dashed lines). Error bars indicate standard errors of the means of all cells.

which enhances Sus protein expression (16) but does not require digestion prior to import and is not highly polymeric, did not enhance protein colocalization as much as amylopectin, which must be degraded to enter the bacterial cell. This observation was very prominent between SusG and SusD or -F ($P < 0.02$), suggesting that the observed protein colocalization in amylopectin is not due to random Sus protein localization but rather is specifically due to starch-induced complex assembly. As expected, colocalization between SusG-HTL and SusG-Ab, i.e., of two markers on the same protein, was the greatest irrespective of the sugar source.

Sus OMP assembly was further evaluated by analyzing the cross-correlation between reconstructed superresolution images of SusG-HTL and Sus-Ab that had been separately reconstructed from single-molecule localizations with <20-nm precision. The cross-correlation function, $c(r)$, measures the increased probability of finding a localized SusG-HTL molecule a distance r away from a localized Sus-Ab molecule. By fitting each cross-correlation curve to an exponential decay, the degree of colocalization between SusG-HTL and each Sus-Ab, and the nanometer-scale size of the colocalized clusters, were defined by an amplitude (A) and a correlation length (ξ), respectively (30, 31). Consistent with the Pearson and Manders coefficients, we observed low amplitudes that indicate only moderate colocalization of SusG with SusD, -E, and -F in glucose. This implies that SusG only weakly interacts with other Sus proteins in the absence of starch, which may expedite processing when starch becomes available. However, amylopectin enhanced Sus protein colocalization for all three pairs, as implied by higher cross-correlation amplitudes (Fig. 3G to I; also, see Table S1A in the supplemental material). This starch-induced clustering was most prominent between SusG and -D ($P < 0.02$). Although starch-induced OMP assembly is evident from this analysis, it is important to note that we measured a lower limit of colocalization that would not include any small amount of unlabeled SusG. Also in agreement with the correlation coefficients, the amplitude of the cross-correlation between HaloTag and antibody labels both on SusG was not enhanced in amylopectin and maltose compared to glucose (see Fig. S2G in the supplemental material). Interestingly, all Sus protein pairs exhibited ~50-nm lengths for SusG-HTL and Sus-Ab protein clusters regardless of the sugar source or the Ab-labeled Sus protein (ξ in Table S1A in the supplemental material).

B. thetaiotaomicron can express 88 different gene clusters to process various glycans by forming Sus-like systems (17, 32). To verify that the observed Sus OMP colocalization is the result of specific interactions among Sus proteins, SusG-HTL and an Ab-labeled SusD-like protein specific for pectic galactan (PG-D) were simultaneously monitored using amylopectin and pectic galactan as sugar sources (33). Although fluorescence imaging indicates that both starch and pectic galactan utilization systems can be expressed simultaneously in *B. thetaiotaomicron*, we observed no significant colocalization between SusG and PG-D compared to SusG and SusD (see Fig. S2H to J in the supplemental material).

To further test our hypothesis that Sus proteins cluster in the presence of starch, random membrane protein localizations on the outer membrane of a *B. thetaiotaomicron* cell were simulated in MATLAB, generating red and green foci corresponding to SusG-HTL and Sus-Ab, respectively. These Monte Carlo simulations confirmed that random colocalization contributes only minimally to the Manders coefficients and is not detected in the cross-correlation analysis. Furthermore, M_{red} and M_{green} depend only weakly on the number of proteins within the experimentally observed range (~10 to 15 protein foci/cell) (Fig. 4A and B). Next, we investigated the effect of microscope focus region on random protein localization. Regardless of whether the microscope focus encompassed the whole cell or a single side of the membrane, apparent protein colocalization was not significantly affected by the microscope focus (Fig. 4C and D). In contrast to random protein localization, we were able to reproduce the experimentally observed protein colocalization using simulated colocalized data with ~50-nm cluster lengths (Fig. 4E and F). These simulations support our conclusion that the measured colocalization is a consequence of starch-induced Sus OMP assembly.

Starch confines SusG motion. The protein diffusion rate is inversely proportional to the size of the protein or protein complex. Accordingly, changes in mobility can provide insight into how an individual protein associates with other proteins in cells. To provide a baseline for interactions between SusG and other Sus OMPs, the dynamic behavior of SusG was characterized by live-cell imaging of SusG-HTL in glucose (see Movies S1 and S2 in the supplemental material). Single-molecule trajectories demonstrating the movement of individual proteins on the membrane were obtained by tracking localized molecules (Fig. 5A) (34). The observed mean square displacement (MSD) slopes of individual trajectories revealed the presence of at least two distinct SusG populations (Fig. 5B): mobile (red) and confined (blue). In glucose, the mobile population predominated, suggesting that SusG tends to diffuse freely along the cell membrane during growth in this simple sugar.

To explore SusG/starch interactions during carbohydrate degradation, two-color single-molecule experiments were performed using Alexa 488-labeled maltoheptaose (MH-Alexa 488) or amylopectin (AP-Alexa 488) in live *B. thetaiotaomicron* (see Fig. S3A to C in the supplemental material) (35, 36). Single-molecule SusG-HTL trajectories clearly show dynamic interactions between SusG and starch molecules (Fig. 5E; also, see Fig. S3E and Movie S3 in the supplemental material), and single-step analysis of SusG-HTL shows a preponderance of very small steps at the AP-Alexa 488 location (Fig. 5G). Of steps that are <50 nm in size, 81% were located within 100 nm of starch. For detailed analysis of these interactions, MSDs were obtained from SusG-HTL molecular tracks in the presence of fluorophore-labeled amylopectin or maltoheptaose. In contrast to the predominantly freely diffusing SusG observed in glucose (Fig. 5B), the presence of starch increased the proportion of confined SusG molecules (blue curves in Fig. 5F and in Fig. S3G in the supplemental material). Since both fluorophore-labeled sugars attached to *B. thetaiotaomicron* did not show any detectable movements within the experimental observation time (Fig. 5C and D; also, see Fig. S3D and F in the supplemental material), we attribute the confined SusG population to direct interactions between sugars and SusG, either alone or complexed with other Sus OMPs. The large amylopectin was multiply labeled and easily observed (see Fig. S3C). Therefore, AP-Alexa 488 was used to characterize dynamic interactions between SusG and starch for subsequent analysis.

SusG exhibits multiple diffusion modes. Heterogeneous motion of SusG-HTL implies the presence of multiple diffusion modes, even within the trajectory of a single SusG protein (Fig. 6). In addition to an immobile state, real-time movement of SusG on the membrane indicates the presence of at least two mobile states, slow (cyan) and fast (red). To extract the two corresponding dif-

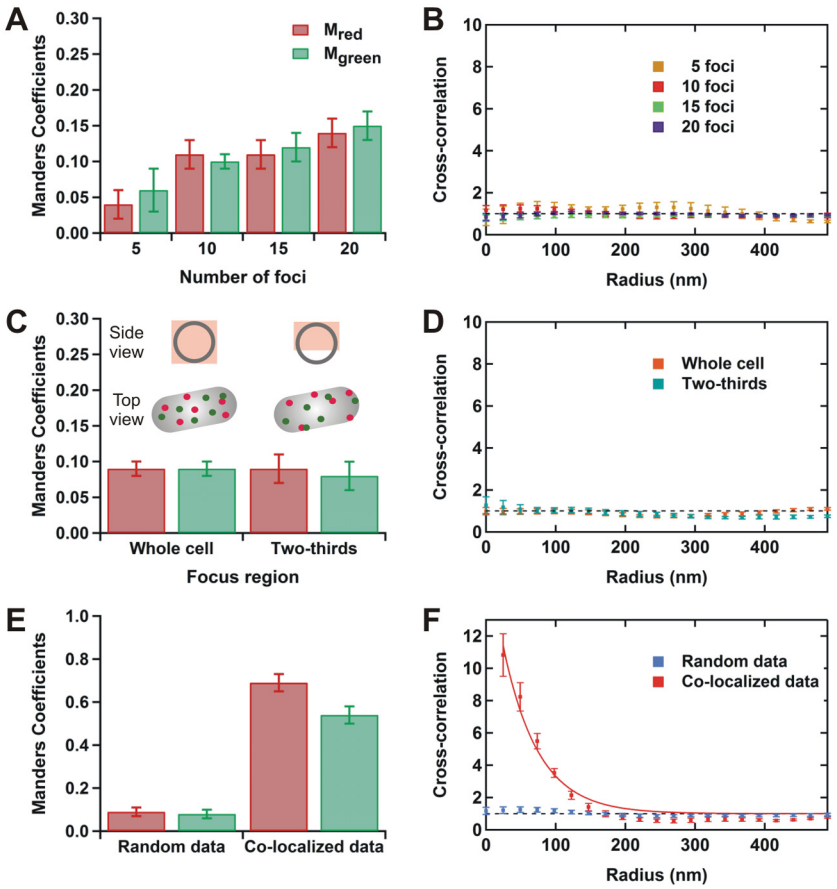

FIG 4 Simulations of membrane protein localizations. (A) Manders coefficients (M_{red} and M_{green}) and (B) cross-correlation demonstrating the effect of number of foci on random protein colocalization. (C and D) Manders coefficients and cross-correlation showing the effect of focus region on random protein colocalization. (C, inset) Schematic representation of the focus region and the top view of the corresponding cell with red and green foci represent the HaloTag-labeled SusG and antibody-labeled Sus proteins, respectively. (E) Comparison of simulated random versus simulated colocalized (within 50 nm) protein distributions by Manders coefficients and (F) corresponding comparison of cross-correlation. Error bars indicate standard errors of the means obtained for 20 simulated cells.

fusion coefficients (D), single-step analysis was performed, fitting the cumulative probability distribution (CPD) of all the squared step sizes to different multiterm exponential functions (see Fig. S4 in the supplemental material). Based on the observed residuals and step sizes (Fig. 6; also, see Fig. S4), a three-term exponential function (see Materials and Methods) was selected as the minimal model to describe the dynamic behavior of SusG (Fig. 7A to D) (34, 37).

In glucose, mobile SusG-HTL predominantly (61%) diffused rapidly (D_{fast} = 0.020 $\mu m^2/s$); we conclude that this fast movement represents the dynamic behavior of individual, freely diffusing SusG molecules. Less frequently (39%), SusG-HTL diffused slowly (D_{slow} = 0.0050 $\mu m^2/s$), possibly due to interactions with one or more other Sus OMPs (Fig. 7A and C; also, see Fig. S5A and Table S1B in the supplemental material). In starch, most SusG-HTL molecules (58%) moved slowly (D_{slow} = 0.0015 $\mu m^2/s$), in contrast to the less frequently observed (42%) fast-moving SusG-HTL molecules (D_{fast} = 0.008 $\mu m^2/s$) (Fig. 7B and D; also, see Fig. S5B and Table S1B). The increased proportion of slow-moving SusG-HTL together with the decreased D_{slow} in starch further supports our model of starch-induced Sus OMP assembly. Consistent with the decreased D_{fast} in starch relative to glucose, stoichiometry determined from the number of photobleaching steps (38) indicates that SusG primarily exists as monomers or dimers in glucose and that it tends to form clusters in the presence of starch (Fig. 7E and F).

In addition to the mobile SusG populations, SusG appeared immobile on the cell membrane ~6 to 7% of the time, both in glucose and in starch. To test for the possibility that this immobile population resulted from interactions between SusG-HTL and the *B. thetaiotaomicron* polysaccharide capsule (39), we monitored SusG-HTL dynamics in capsule-free *B. thetaiotaomicron* (ΔCPS) cells. SusG-HTL in ΔCPS cells behaved similarly to the wild-type in both glucose and amylopectin (see Fig. S5C and D and Table S1B in the supplemental material). Thus, we attribute the immobile populations to interactions between SusG and other membrane components, as well as to artifacts from imaging inherently 3D motion in 2D. Since the fraction of the immobile population remains unchanged in all further analysis, we omit it from further discussion.

Dynamic interactions among Sus proteins. To further elucidate the starch-induced Sus complex assembly mechanism, SusG-HTL diffusion was characterized in Sus protein knockout strains in glucose and starch (8). First, to reveal interactions between

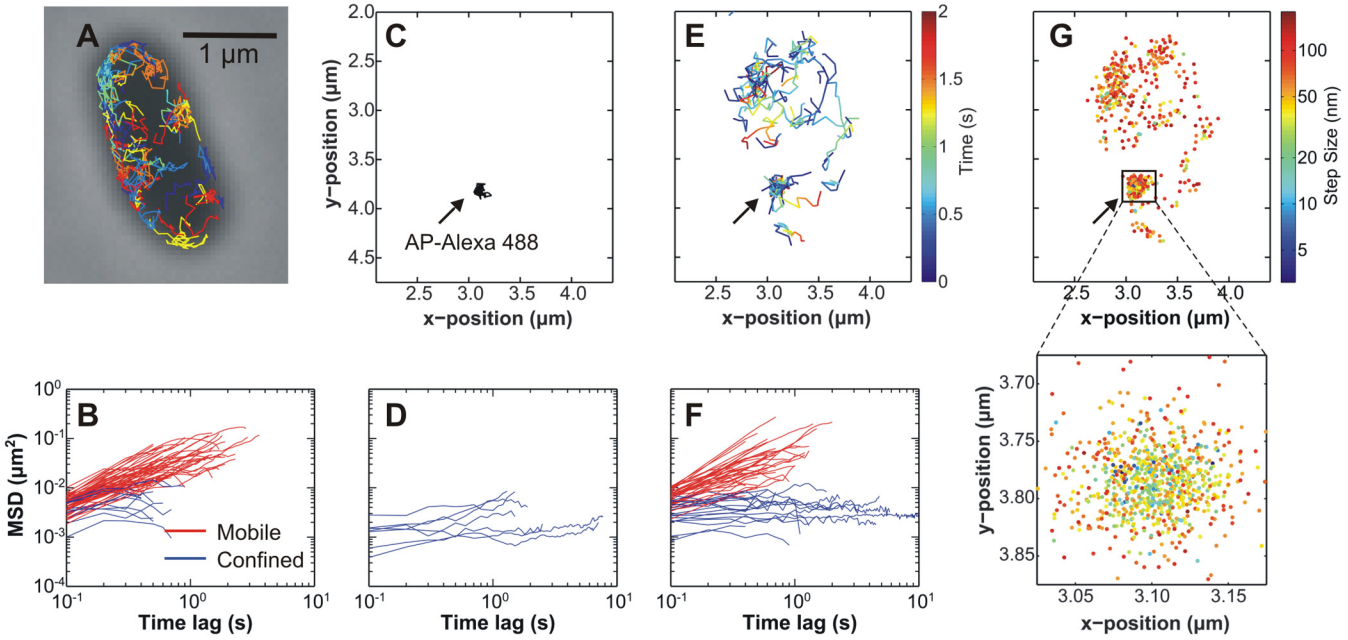

FIG 5 SusG diffuses heterogeneously but is confined in the presence of starch. (A) Single-molecule trajectories of SusG-HTL in glucose (random colors). (B) Mean square displacement (MSD) versus time lag for the tracks observed on the cell in panel A. Based on diffusion coefficients (D), trajectories were categorized into two subpopulations: mobile (red, $D > 0.01$ $\mu m^2/s$) and confined (blue, $D < 0.01$ $\mu m^2/s$). The 0.01-$\mu m^2/s$ cutoff was empirically determined based on the measured distribution of single-molecule diffusion coefficients to distinguish between the two qualitatively observed SusG subpopulations. (C and D) Tracks and MSD plot showing confined movement of Alexa 488-labeled amylopectin (AP-Alexa 488) bound to a cell. (E and F) Time-dependent tracks and MSD plot of SusG-HTL in the presence of AP-Alexa 488 (arrow). (G) Spatial distribution of SusG-HTL step sizes obtained from the tracks in panel E. All data were obtained by imaging at 10 frames per s.

SusG and SusC during starch processing, SusG-HTL dynamics were monitored in *susC* gene knockout cells (Δ*susC*). Although SusC is essential for starch catabolism in *B. thetaiotaomicron*, the absence of SusC did not affect the fast ($D_{fast} = 0.022$ $\mu m^2/s$, 61%) or the slow ($D_{slow} = 0.0055$ $\mu m^2/s$, 39%) SusG-HTL diffusion rates in glucose (see Fig. S5I and Table S1B in the supplemental material).

The roles of SusE and SusF in Sus complex assembly were explored by monitoring SusG-HTL dynamics in *B. thetaiotaomicron* lacking SusE and SusF expression (ΔSusEF) (see Fig. S5G and H and Table S1B in the supplemental material). The loss of SusEF did not alter SusG-HTL diffusion in glucose. Conversely, relative to wild-type cells, in starch, ΔSusEF gave rise to an increased fast-mode population ($D_{fast} = 0.012$ $\mu m^2/s$; 51% for ΔSusEF cells versus 42% for WT cells). This suggests that the Sus complex is destabilized without SusEF. Furthermore, in starch, ΔSusEF *B. thetaiotaomicron* displayed a 2-fold increase in SusG-HTL D_{slow} ($D_{slow} = 0.0030$ $\mu m^2/s$, 49%). This increase in D_{slow}, the diffusion coefficient assigned to the motion of SusG associated with other Sus OMPs, supports the presence of SusE and/or -F in the wild-type complex. Regardless of the observed SusG diffusion differences, colocalization between SusG and SusD was not affected by the absence of SusEF (see Fig. S6 in the supplemental material). This suggests that SusG interacts with SusD independently of SusEF, either by direct interactions or by mutual interactions with starch.

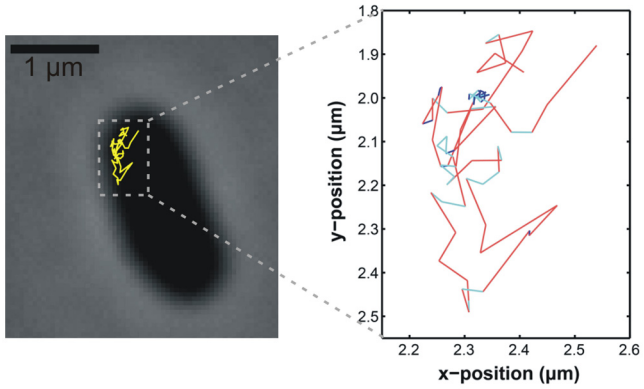

FIG 6 SusG diffuses heterogeneously in live *B. thetaiotaomicron*. A typical SusG-HTL single-molecule trajectory superimposed on the phase-contrast cell image (left) and the enlarged trajectory showing different step sizes of SusG-HTL in glucose (right) are shown. Red indicates large steps (>45 nm), corresponding to the fast-diffusion mode, cyan indicates small steps (20 to 45 nm), corresponding to the slow-diffusion mode, and blue indicates SusG-HTL, which appears immobile within the localization precision (<20 nm).

Finally, to further probe the interaction of SusG and SusD in the presence of starch, SusG-HTL dynamics were monitored in *susD* gene knockout (Δ*susD*) cells. SusG-HTL in Δ*susD* showed dynamics similar to those of wild-type *B. thetaiotaomicron* in glucose (see Fig. S5E and Table S1B in the supplemental material). Furthermore, *susD* knockout had an effect similar to that of SusEF knockout on SusG-HTL dynamics in starch (see Fig. S5F): relative to wild-type cells in starch, the absence of SusD in starch increased D_{slow} for SusG-HTL ($D_{slow} = 0.0037$ $\mu m^2/s$; 52%) and increased the population of fast-moving molecules ($D_{fast} = 0.011$ $\mu m^2/s$; 48%). The enhanced D_{slow} in Δ*susD* cells provides evidence that

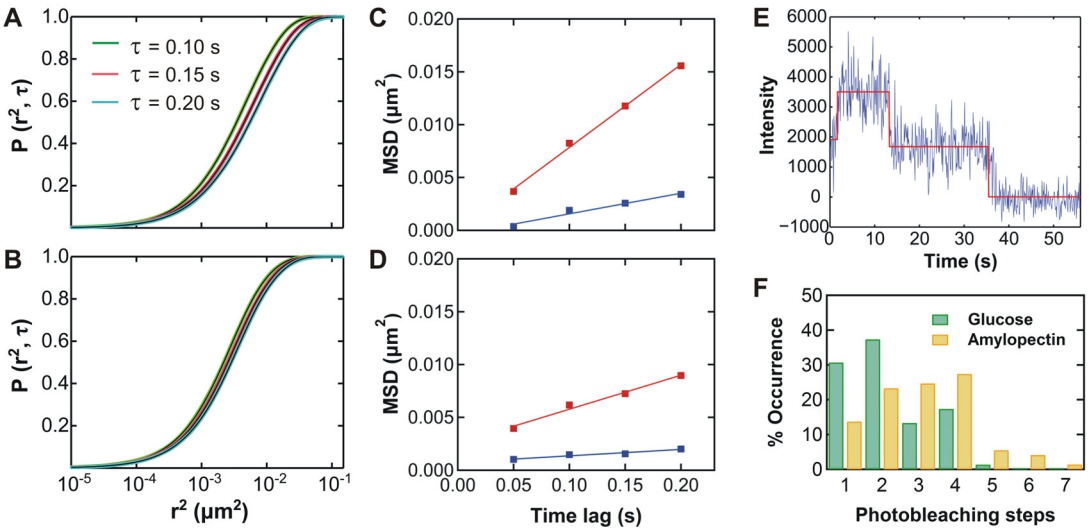

FIG 7 Cumulative probability distribution (CPD) analysis of SusG dynamics and bleaching analysis of SusG stoichiometry. (A and B) Distributions of squared step sizes (r^2) of SusG-HTL fit to a three-term CPD function in glucose and amylopectin, respectively, based on images obtained at 20 frames per s. Raw data (colored lines) and corresponding fits (black lines) were obtained for three different time lags (τ), as indicated. (C and D) MSD versus τ obtained from fitting the CPD curves of SusG-HTL in glucose and amylopectin, respectively. The MSD plot slopes reveal fast (red) and slow (blue) diffusion modes for SusG in live cells. (E) Typical fluorescent intensity trace for TMR-HaloTag-labeled SusG showing multiple photobleaching steps corresponding to several fluorophore-labeled SusG molecules detected in a given focus. The red-line fit was obtained from a change point-finding algorithm (38). (F) Occurrence of the number of photobleaching steps, revealing the approximate cluster size of SusG molecules in glucose and amylopectin.

SusD is also a member of the starch-induced Sus complex. Taken together, the absence of any one or several other Sus OMPs did not influence the overall SusG dynamics in glucose but clearly affected D_{slow} in starch, indicating dynamic associations between SusG and other Sus proteins during starch degradation.

DISCUSSION

Human gut *Bacteroidetes* promote complex glycan digestion in the gut by coordinated actions of membrane-associated protein complexes. The ability of this bacterial group to target a wide variety of polysaccharides makes them key players in this important symbiotic process. Despite their importance to human health, the precise mechanisms by which these proteins perform their functions are still obscure (1, 5). Using the *B. thetaiotaomicron* Sus as a model, we have characterized the assembly and real-time dynamics of these OMPs in live cells. Although Sus proteins were predicted to assemble to process starch, this phenomenon had not previously been directly observed in live bacteria. To reveal interactions among Sus proteins during starch catabolism with high resolution, we employed single-molecule superresolution imaging in live *B. thetaiotaomicron* to detect fluorophore-labeled Sus proteins in real time.

Protein correlation studies performed in fixed cells collectively revealed that simple, nonpolymeric sugars such as glucose and maltose do not induce Sus complex assembly. On the other hand, the presence of large starch molecules enhances Sus protein colocalization in *B. thetaiotaomicron*, suggesting the collaborative degradation of starch by a multicomponent Sus complex. SusG diffusion was slowed in starch compared to glucose, partly due to direct contact with starch itself. However, the loss of one or more Sus OMPs further altered the SusG diffusion rate, suggesting interactions between Sus OMPs in the presence of starch. Taking these data together, we propose a model in which starch-induced Sus OMP complex assembly promotes starch processing in live *B. thetaiotaomicron* (Fig. 8). Our dynamic model fits well with existing knowledge of other *Bacteroidetes* Sus-like systems, which exhibit increasing numbers of OMPs (both enzymes and binding proteins) as polysaccharide linkage complexity increases (40). Since protein complex formation is primarily linked to substrate, more complex Sus-like systems can evolve to incorporate additional OMP functions in the form of freely diffusing OM lipoproteins that need not fit into a more precisely arranged protein complex.

Interestingly, none of our Sus protein knockouts affected the SusG diffusion rates in glucose. Consistent with our proposed model, these data suggest that the observed moderate protein colocalization in glucose results from transient interactions among Sus proteins on the membrane. In starch, the absence of SusD or SusEF increased the overall diffusion rate of SusG, suggesting that at least a single copy of these proteins plays a role in starch-induced Sus OMP complex. In addition to the change in diffusion rates, a decrease in the proportion of slow-moving SusG in starch implies that the absence of one or more Sus proteins may decrease the overall complex stability.

The carbohydrate environment in the gut is constantly changing, making it critical for gut bacteria to rapidly sense and respond to available glycans. Starch-induced assembly of the Sus complex on the membrane is an apt approach for efficient starch processing in *B. thetaiotaomicron*. This dynamic process allows Sus OMPs to transition from a rapidly diffusing "surveillance" state in the absence of starch to a complex that can efficiently capture, degrade, and import glycans into the cell from a single locus when the target substrate becomes available. SusG partitioning between slow and fast modes suggests that even in the presence of starch, the interaction of SusG and other Sus proteins is dynamic. Perhaps SusG disengagement from both starch and other Sus proteins provides

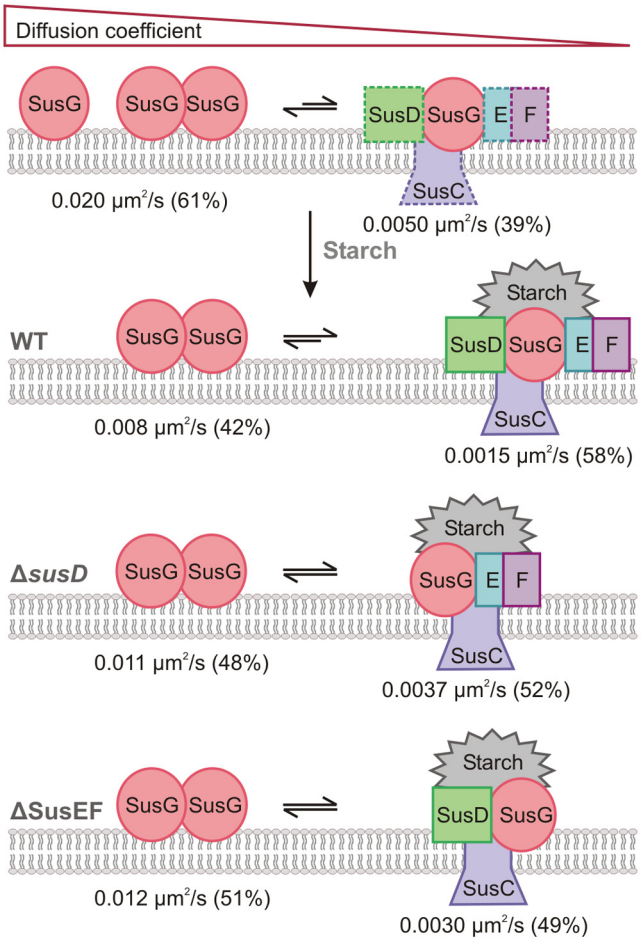

FIG 8 Model for starch-induced assembly of the Sus complex. In the absence of starch, SusG predominantly exists as fast-diffusing free molecules (left) rather than as slow-moving SusG molecules that are in complex with one or more other Sus partners (dashed lines, right). In the presence of starch, interactions between starch and Sus proteins increase the slow-moving SusG population due to starch-induced Sus complex assembly. This complex diffuses faster in Δ*susD* and ΔSusEF cells, indicating the presence of SusD and of SusE and/or SusF in the Sus OMP complex.

both the substrate and the other Sus proteins additional degrees of freedom to facilitate malto-oligosaccharide import. The dynamic assembly we observed for *B. thetaiotaomicron* Sus OMP-mediated starch degradation suggests a general mechanism by which many other Sus-like systems may operate in gut bacteria. If so, our real-time observations of Sus OMP dynamics during starch catabolism and our protein correlation analysis not only provide insight into how this multiprotein system works in live *B. thetaiotaomicron* but also will pave the way to understanding myriad Sus-like systems in other human gut symbionts.

MATERIALS AND METHODS

Bacterial growth conditions and genetic manipulation. *B. thetaiotaomicron* was grown at 37°C under anaerobic conditions in medium containing tryptone-yeast extract-glucose (TYG) and diluted into minimal medium containing 0.5% (wt/vol) carbohydrate source (17). To monitor protein expression in the presence of maltose or maize amylopectin, cells at mid-log to late log phase in minimal medium containing glucose were incubated for 10 min in fresh, prereduced medium containing glucose and the appropriate sugar (glucose-maltose or glucose-amylopectin, ~5:1) (33). Genetic manipulation of *B. thetaiotaomicron* was achieved using a counterselectable allelic exchange method as previously described (10).

HaloTag labeling of SusG. A construct with *B. thetaiotaomicron* SusG fused to a HaloTag protein (SusG-HT) was made by replacing CBM58 of SusG (residues 219 to 336) with the HaloTag protein (inactive haloalkane dehalogenase) (14, 24). Although the CBM58 domain of SusG enhances the binding of SusG to insoluble starch, we have previously shown that CBM58 is dispensable without loss of SusG catalytic activity in the presence of soluble starch (14). Because *B. thetaiotaomicron* SusG is tethered to the cell membrane via lipidation of an N-terminal Cys that follows the signal peptide, and because the structure of CBM58 is inconsistent with a dual role in binding both starch and the capsular polysaccharide, we do not expect the CBM58 deletion to affect SusG function. *B. thetaiotaomicron* expressing SusG-HT at the native promoter was labeled with HaloTag tetramethyl rhodamine (TMR) ligand (5 μM; Promega) by incubation for 10 to 15 min at 37°C in the dark as recommended by the manufacturer. To remove excess dye, cells were washed once with phosphate-buffered saline (PBS) buffer (pH 7.5) followed by two 10-min incubations in PBS at 37°C. Cells were then incubated in 1× minimal medium-PBS for 30 min at 37°C, followed by resuspension in fresh minimal medium containing the appropriate sugar for live-cell imaging. The labeled cells were compared to mock-treated cells that had been prepared as described above but incubated in minimal medium (1×, no carbohydrate source) rather than in a HaloTag TMR ligand solution. Fluorescent labeling of SusG-HT with the HaloTag TMR ligand does not significantly affect the growth rate in amylopectin compared to mock-treated cells (doubling time of TMR-HT treated cells = 56.4 ± 3.0 min; that of mock-treated cells = 56.9 ± 5.3 min; $P = 0.85$). For fixed-cell imaging, cells were further incubated in 4% paraformaldehyde for 15 min and washed twice with PBS at room temperature before being resuspended in fresh minimal medium-PBS. Under the optimized labeling conditions, we observed no nonspecific fluorophore binding in ~70% of *B. thetaiotaomicron* cells expressing wild-type SusG instead of SusG-HT and very few, short-lived nonspecific labels in the other ~30% of these control cells.

Antibody labeling of Sus proteins. To monitor Sus proteins on the cell surface, formaldehyde-fixed nonpermeabilized *B. thetaiotaomicron* cells were blocked in PBS containing 2% goat serum and incubated with rabbit polyclonal antibodies (Cocalico Biologicals) specific to individual Sus proteins. After being washed with PBS, the cells were incubated in Alexa 488-conjugated goat anti-rabbit IgG secondary antibodies (Molecular Probes). Antibody-labeled cells were rinsed several times with PBS and resuspended in minimal medium for cellular imaging. For protein colocalization experiments, cells were labeled with the HaloTag TMR ligand and fixed with formaldehyde prior to antibody labeling.

Superresolution imaging of live bacterial cells. For live-cell imaging, fluorophore-labeled cells were incubated in fresh medium for 30 min at 37°C in the anaerobic chamber before imaging. Both fixed and live fluorophore-labeled *B. thetaiotaomicron* cells were deposited in minimal medium containing a carbohydrate source and a reducing agent onto pads of 2% agarose in the same medium for superresolution imaging. The coverslip edges were sealed with 5 Minute epoxy (Devcon) to maintain an oxygen-free environment (see Fig. S1E in the supplemental material) (26). *B. thetaiotaomicron* cells were imaged on an Olympus IX71 inverted fluorescence microscope equipped with a 1.40 numerical aperture (NA), 100× oil immersion wide-field phase-contrast objective or a 1.49 NA, 100× oil immersion total internal fluorescence (TIRF) objective (Olympus). *B. thetaiotaomicron* containing SusG labeled with the HaloTag TMR ligand (SusG-HTL) and Alexa 488-conjugated antibody-labeled Sus proteins was excited with 561-nm (Coherent Sapphire 561-50) and 488-nm (Coherent Sapphire 488-50) lasers for the respective labels. Fluorescence emission intensities were detected on a 512- by 512-pixel Photometrics Evolve electron-multiplying charge-coupled device (EMCCD) camera at 10 to 20 frames per s in fixed and live cells with appropriate filters (41).

CPD analysis was performed using images obtained at 20 frames per s in live cells. TetraSpeck fluorescent microspheres (Molecular Probes) were used as markers to correct chromatic aberrations during imaging. The microspheres also served as fiducial markers to correct for subtle stage drift. To monitor protein dynamics under native conditions, live bacterial cells were imaged at 37°C in the presence of glucose or fluorophore-labeled carbohydrates using an objective heater (Bioptechs).

Fluorophore labeling of carbohydrates. Maltoheptaose (Sigma-Aldrich) was fluorophore-labeled at the reducing end using a 1:0.2:1.2 molar ratio of maltoheptaose, Alexa 488 hydrazide (Molecular Probes), and 2-picoline borane (Sigma-Aldrich) (35). During the labeling reaction, maltoheptaose was first dissolved in a 1:3 water-methanol mixture containing 2.5% (vol/vol) acetic acid and incubated with Alexa 488 hydrazide at 65°C in the dark. After 30 min of incubation, 2-picoline borane was added to the reaction mixture, which was further incubated at 65°C for 45 min. To remove unbound fluorophores, the reaction mixture was purified using a Sephadex G-10 column (PD MiniTrap G-10; GE Healthcare) followed by high-pressure liquid chromatography (HPLC) with a C_{18} reversed-phase column.

To label amylopectin with fluorescent probes, 100 μl of 10 mg/ml amylopectin from maize (Sigma-Aldrich) was oxidized by 1 μl of 25 mM sodium periodate (Sigma-Aldrich) for 60 min at room temperature (36). The reaction was stopped by addition of 5 μl ethylene glycol. Oxidized amylopectin was fluorophore labeled using 2 μl of 17.5 mM Alexa 488 hydrazide by incubation at 65°C for 30 min. After addition of 2 μl of 100 mM 2-picoline borane, the reaction mixture was further incubated for 60 min at 65°C to perform reductive amination (35). The excess dye was removed with a Sephadex G-25 column (PD SpinTrap G-25; GE Healthcare).

Image processing. Stacked images were analyzed by fitting the point spread function of isolated single molecules in each imaging frame to a 2D symmetric Gaussian function to localize the emitter positions using the MATLAB nonlinear least-squares regression function *nlinfit* (27). Superresolution images were reconstructed from these positions by plotting each localized fit as a 2D Gaussian function with constant intensity and with a standard deviation equal to the statistical localization precision (95% confidence interval on the position).

Sus protein colocalization was analyzed by computing two pixel intensity-based quantities: Pearson's correlation coefficient (r) and the Manders coefficients (M_{red} and M_{green}) (29).

$$r = \frac{\sum \left(R_i - \overline{R}\right) \times \left(G_i - \overline{G}\right)}{\sqrt{\sum \left(R_i - \overline{R}\right)^2 \times \sum \left(G_i - \overline{G}\right)^2}}$$

$$M_{red} = \frac{\sum_i R_{i,coloc}}{\sum_i R_i}$$

$$M_{green} = \frac{\sum_i G_{i,coloc}}{\sum_i G_i}$$

For pixel i in the images, R and G are intensities of the red and the green channels, respectively. $R_{i,coloc}$ and $G_{i,coloc}$ represent intensities of red and green pixels that also have the other component. These coefficients were obtained using standard ImageJ plugins to analyze reconstructed superresolution images of the red (TMR) and green (Alexa 488) channels corresponding to SusG-HTL and antibody-labeled Sus proteins, respectively. Sus protein colocalization was quantified by analyzing the cross-correlation functions between different protein pairs obtained by comparing reconstructed superresolution images with fast Fourier transforms in MATLAB (30). Cross-correlation was performed on a whole bacterial cell mask determined from the reconstructed images.

Single-molecule tracking was performed using a custom MATLAB code that determines molecular trajectories as a function of time. Single-molecule tracks were constructed by connecting molecules that are localized in consecutive frames within 150 nm for a minimum of 0.7 s. The density of fluorophore-labeled proteins per frame was kept low (1 to 3 molecules/cell) to ensure accurate tracking of mobile molecules. Diffusion coefficients of individual SusG trajectories were obtained from the slopes of the first 2/3 data points of corresponding MSD curves.

CPD analysis. Ensemble MSDs were found for every time lag (time interval between positions, τ) by fitting the cumulative probability distribution of the squared step sizes to a three-term exponential function consisting of one immobile and two mobile terms that best describe the data (see Fig. S4 in the supplemental material) (34, 37).

$$P(U,\tau) = 1 - \left[\alpha \cdot \exp\left(\frac{-U}{\langle r_1^2(\tau)\rangle + \sigma^2}\right) + \beta \cdot \exp\left(\frac{-U}{\langle r_2^2(\tau)\rangle + \sigma^2}\right) + \gamma \cdot \exp\left(\frac{-U}{\sigma^2}\right)\right]$$

where $P(U, \tau)$ denotes the probability that the squared displacement (r^2) for a given time (τ) does not exceed the specific value U. The coefficients α, β, and γ indicate the fractions of molecules in the fast, slow, and immobile modes, respectively, at any given time within the localization precision (σ), and $\alpha + \beta + \gamma = 1$. The average SusG diffusion coefficient for each mode was determined from the linear slope of MSD versus τ for the first four τ values (42).

Monte Carlo simulations. To support protein colocalization results, membrane protein localization was further studied using data generated in MATLAB to simulate random cell surface localizations. The *B. thetaiotaomicron* cell was modeled as a cylinder (length, 1.5 μm; radius, 0.5 μm) with 0.5-μm radius hemispheric caps. The MATLAB function *random* was used to generate a specified number (5 to 20) of random simulated localizations of each color (red and green) according to a uniform distribution on the cell surface. The intensity and width of each data point were randomly selected according to a normal distribution about the experimental averages. The effect of focal plane position was investigated by constraining the localizations in the axial direction to the whole cell and to the top 0.67 μm of the cell. For simulated colocalized data, the MATLAB function *randsample* was used to distribute red points according to a normal distribution (σ = 50 nm) about each randomly generated green point by using the MATLAB weighting function *rowweight*.

SUPPLEMENTAL MATERIAL

Supplemental material for this article may be found at http://mbio.asm.org/lookup/suppl/doi:10.1128/mBio.02172-14/-/DCSupplemental.

Movie S1, AVI file, 3.9 MB.
Movie S2, AVI file, 4.5 MB.
Movie S3, AVI file, 5 MB.
Figure S1, TIF file, 8.9 MB.
Figure S2, TIF file, 8.9 MB.
Figure S3, TIF file, 7.9 MB.
Figure S4, TIF file, 9.3 MB.
Figure S5, TIF file, 12.8 MB.
Figure S6, TIF file, 4.6 MB.
Table S1, DOC file, 0.1 MB.

ACKNOWLEDGMENTS

This work was supported by a Burroughs Wellcome Career Award at the Scientific Interface to J.S.B. and a University of Michigan MCubed award to J.S.B., N.M.K. and E.C.M. E.A.C. was supported by the NIH-sponsored University of Michigan Genetics Training Program (GM07544).

We thank Sarah Veatch and Yi Liao for their help implementing the cross-correlation and cumulative probability data analyses.

REFERENCES

1. **Koropatkin NM, Cameron EA, Martens EC.** 2012. How glycan metabolism shapes the human gut microbiota. Nat. Rev. Microbiol. **10:**323–335. http://dx.doi.org/10.1038/nrmicro2746.
2. **Bäckhed F, Ley RE, Sonnenburg JL, Peterson DA, Gordon JI.** 2005. Host-bacterial mutualism in the human intestine. Science **307:**1915–1920. http://dx.doi.org/10.1126/science.1104816.

3. **McNeil NI.** 1984. The contribution of the large-intestine to energy supplies in man. Am. J. Clin. Nutr. **39:**338–342.
4. **Sonnenburg JL, Xu J, Leip DD, Chen CH, Westover BP, Weatherford J, Buhler JD, Gordon JI.** 2005. Glycan foraging *in vivo* by an intestine-adapted bacterial symbiont. Science **307:**1955–1959. http://dx.doi.org/10.1126/science.1109051.
5. **Martens EC, Koropatkin NM, Smith TJ, Gordon JI.** 2009. Complex glycan catabolism by the human gut microbiota: the Bacteroidetes Sus-like paradigm. J. Biol. Chem. **284:**24673–24677. http://dx.doi.org/10.1074/jbc.R109.022848.
6. **Salyers AA, Vercellotti JR, West SE, Wilkins TD.** 1977. Fermentation of mucin and plant polysaccharides by strains of Bacteroides from the human colon. Appl. Environ. Microbiol. **33:**319–322.
7. **Tancula E, Feldhaus MJ, Bedzyk LA, Salyers AA.** 1992. Location and characterization of genes involved in binding of starch to the surface of *Bacteroides thetaiotaomicron*. J. Bacteriol. **174:**5609–5616.
8. **Anderson KL, Salyers AA.** 1989. Genetic evidence that outer membrane binding of starch is required for starch utilization by *Bacteroides thetaiotaomicron*. J. Bacteriol. **171:**3199–3204.
9. **Cho KH, Salyers AA.** 2001. Biochemical analysis of interactions between outer membrane proteins that contribute to starch utilization by *Bacteroides thetaiotaomicron*. J. Bacteriol. **183:**7224–7230. http://dx.doi.org/10.1128/JB.183.24.7224-7230.2001.
10. **Koropatkin NM, Martens EC, Gordon JI, Smith TJ.** 2008. Starch catabolism by a prominent human gut symbiont is directed by the recognition of amylose helices. Structure **16:**1105–1115. http://dx.doi.org/10.1016/j.str.2008.03.017.
11. **Shipman JA, Berleman JE, Salyers AA.** 2000. Characterization of four outer membrane proteins involved in binding starch to the cell surface of *Bacteroides thetaiotaomicron*. J. Bacteriol. **182:**5365–5372. http://dx.doi.org/10.1128/JB.182.19.5365-5372.2000.
12. **Cameron EA, Maynard MA, Smith CJ, Smith TJ, Koropatkin NM, Martens EC.** 2012. Multidomain carbohydrate-binding proteins involved in *Bacteroides thetaiotaomicron* starch metabolism. J. Biol. Chem. **287:**34614–34625. http://dx.doi.org/10.1074/jbc.M112.397380.
13. **Shipman JA, Cho KH, Siegel HA, Salyers AA.** 1999. Physiological characterization of SusG, an outer membrane protein essential for starch utilization by *Bacteroides thetaiotaomicron*. J. Bacteriol. **181:**7206–7211.
14. **Koropatkin NM, Smith TJ.** 2010. SusG: A unique cell-membrane-associated alpha-amylase from a prominent human gut symbiont targets complex starch molecules. Structure **18:**200–215. http://dx.doi.org/10.1016/j.str.2009.12.010.
15. **D'Elia JN, Salyers AA.** 1996. Contribution of a neopullulanase, a pullulanase, and an alpha-glucosidase to growth of *Bacteroides thetaiotaomicron* on starch. J. Bacteriol. **178:**7173–7179.
16. **D'Elia JN, Salyers AA.** 1996. Effect of regulatory protein levels on utilization of starch by *Bacteroides thetaiotaomicron*. J. Bacteriol. **178:**7180–7186.
17. **Martens EC, Chiang HC, Gordon JI.** 2008. Mucosal glycan foraging enhances fitness and transmission of a saccharolytic human gut bacterial symbiont. Cell Host Microbe **4:**447–457. http://dx.doi.org/10.1016/j.chom.2008.09.007.
18. **Fernández-Suárez M, Ting AY.** 2008. Fluorescent probes for super-resolution imaging in living cells. Nat. Rev. Mol. Cell Biol. **9:**929–943. http://dx.doi.org/10.1038/nrm2531.
19. **Chudakov DM, Matz MV, Lukyanov S, Lukyanov KA.** 2010. Fluorescent proteins and their applications in imaging living cells and tissues. Physiol. Rev. **90:**1103–1163. http://dx.doi.org/10.1152/physrev.00038.2009.
20. **Biteen JS, Moerner WE.** 2010. Single-molecule and superresolution imaging in live bacteria cells. Cold Spring Harb. Perspect. Biol. **2:**a000448. http://dx.doi.org/10.1101/cshperspect.a000448.
21. **Huang B, Babcock H, Zhuang X.** 2010. Breaking the diffraction barrier: super-resolution imaging of cells. Cell **143:**1047–1058. http://dx.doi.org/10.1016/j.cell.2010.12.002.
22. **Remington SJ.** 2006. Fluorescent proteins: maturation, photochemistry and photophysics. Curr. Opin. Struct. Biol. **16:**714–721. http://dx.doi.org/10.1016/j.sbi.2006.10.001.
23. **Los GV, Wood K.** 2007. The HaloTag: a novel technology for cell imaging and protein analysis. Methods Mol. Biol. **356:**195–208.
24. **Los GV, Encell LP, McDougall MG, Hartzell DD, Karassina N, Zimprich C, Wood MG, Learish R, Ohana RF, Urh M, Simpson D, Mendez J, Zimmerman K, Otto P, Vidugiris G, Zhu J, Darzins A, Klaubert DH, Bulleit RF, Wood KV.** 2008. HaloTag: a novel protein labeling technology for cell imaging and protein analysis. ACS Chem. Biol. **3:**373–382. http://dx.doi.org/10.1021/cb800025k.
25. **Wombacher R, Cornish VW.** 2011. Chemical tags: applications in live cell fluorescence imaging. J. Biophotonics. **4:**391–402. http://dx.doi.org/10.1002/jbio.201100018.
26. **Karunatilaka KS, Coupland BR, Cameron EA, Martens EC, Koropatkin NM, Biteen JS.** 2013. Single-molecule imaging can be achieved in live obligate anaerobic bacteria. Proc. SPIE **8590:**85900K–1–85900K–7. http://dx.doi.org/10.1117/12.2001157.
27. **Biteen JS, Thompson MA, Tselentis NK, Bowman GR, Shapiro L, Moerner WE.** 2008. Super-resolution imaging in live *Caulobacter crescentus* cells using photoswitchable EYFP. Nat. Methods **5:**947–949.
28. **Manders EM, Stap J, Brakenhoff GJ, van Driel R, Aten JA.** 1992. Dynamics of three-dimensional replication patterns during the S-phase, analysed by double labelling of DNA and confocal microscopy. J. Cell Sci. **103**(3):857–862.
29. **Bolte S, Cordelières FP.** 2006. A guided tour into subcellular colocalization analysis in light microscopy. J. Microsc. **224:**213–232. http://dx.doi.org/10.1111/j.1365-2818.2006.01706.x.
30. **Veatch SL, Machta BB, Shelby SA, Chiang EN, Holowka DA, Baird BA.** 2012. Correlation functions quantify super-resolution images and estimate apparent clustering due to over-counting. PLoS One **7:**e31457. http://dx.doi.org/10.1371/journal.pone.0031457.
31. **Sengupta P, Jovanovic-Talisman T, Skoko D, Renz M, Veatch SL, Lippincott-Schwartz J.** 2011. Probing protein heterogeneity in the plasma membrane using PALM and pair correlation analysis. Nat. Methods **8:**969–975. http://dx.doi.org/10.1038/nmeth.1704.
32. **Xu J, Bjursell MK, Himrod J, Deng S, Carmichael LK, Chiang HC, Hooper LV, Gordon JI.** 2003. A genomic view of the human-*Bacteroides thetaiotaomicron* symbiosis. Science **299:**2074–2076. http://dx.doi.org/10.1126/science.1080029.
33. **Rogers TE, Pudlo NA, Koropatkin NM, Bell JS, Moya Balasch M, Jasker K, Martens EC.** 2013. Dynamic responses of *Bacteroides thetaiotaomicron* during growth on glycan mixtures. Mol. Microbiol. **88:**876–890. http://dx.doi.org/10.1111/mmi.12228.
34. **Liao Y, Yang SK, Koh K, Matzger AJ, Biteen JS.** 2012. Heterogeneous single-molecule diffusion in one-, two-, and three-dimensional microporous coordination polymers: directional, trapped, and immobile guests. Nano Lett. **12:**3080–3085. http://dx.doi.org/10.1021/nl300971t.
35. **Ruhaak LR, Steenvoorden E, Koeleman CA, Deelder AM, Wuhrer M.** 2010. 2-Picoline-borane: a non-toxic reducing agent for oligosaccharide labeling by reductive amination. Proteomics **10:**2330–2336. http://dx.doi.org/10.1002/pmic.200900804.
36. **Stephen TL, Fabri M, Groneck L, Röhn TA, Hafke H, Robinson N, Rietdorf J, Schrama D, Becker JC, Plum G, Krönke M, Kropshofer H, Kalka-Moll WM.** 2007. Transport of Streptococcus pneumoniae capsular polysaccharide in MHC class II tubules. PLoS Pathog. **3:**e32. http://dx.doi.org/10.1371/journal.ppat.0030032.
37. **Sonnleitner A, Schütz GJ, Schmidt T.** 1999. Free brownian motion of individual lipid molecules in biomembranes. Biophys. J. **77:**2638–2642. http://dx.doi.org/10.1016/S0006-3495(99)77097-9.
38. **Watkins LP, Yang H.** 2005. Detection of intensity change points in time-resolved single-molecule measurements. J. Phys. Chem. B **109:**617–628. http://dx.doi.org/10.1021/jp0467548.
39. **Martens EC, Roth R, Heuser JE, Gordon JI.** 2009. Coordinate regulation of glycan degradation and polysaccharide capsule biosynthesis by a prominent human gut symbiont. J. Biol. Chem. **284:**18445–18457. http://dx.doi.org/10.1074/jbc.M109.008094.
40. **Martens EC, Lowe EC, Chiang H, Pudlo NA, Wu M, McNulty NP, Abbott DW, Henrissat B, Gilbert HJ, Bolam DN, Gordon JI.** 2011. Recognition and degradation of plant cell wall polysaccharides by two human gut symbionts. PLoS Biol. **9:**e1001221. http://dx.doi.org/10.1371/journal.pbio.1001221.
41. **Moerner WE, Fromm DP.** 2003. Methods of single-molecule fluorescence spectroscopy and microscopy. Rev. Sci. Instrum. **74:**3597–3619. http://dx.doi.org/10.1063/1.1589587.
42. **Michalet X.** 2011. Mean square displacement analysis of single-particle trajectories with localization error: Brownian motion in an isotropic medium. Phys. Rev. E Stat. Nonlin. Soft Matter Phys. **82:**041914. http://dx.doi.org/10.1103/PhysRevE.82.041914.